PROCEEDINGS OF SCIENCE

Fine-Grained Tracker as a Near Detector for LBNE

Xinchun Tian*, **Sanjib Mishra, Roberto Petti and Duyang Hongyue**
University of South Carolina
E-mail: tianxc@gmail.com

The reference design of the near detector for the LBNE experiment is a high-resolution Fine-Grained Tracker (FGT) capable of precisely measuring all four species of neutrinos: ν_μ, ν_e, $\bar{\nu}_\mu$ and $\bar{\nu}_e$. The FGT is composed of a Straw-Tube Tracker (STT) with transition-radiation capability surrounded by a high resolution electromagnetic calorimeter (ECAL) and embedded in a dipole magnet. Muon-ID detectors instrument the iron-yoke of the magnet and the downstream and upstream stations outside the magnet. The STT is instrumented with Ar and other nuclear targets. The goals of the FGT is to constrain the systematic errors, below the corresponding statistical error in the far detector, for all oscillation studies; and to conduct a panoply of precision measurements and searches in Neutrino physics. We present sensitivity studies – critical to constraining the systematics in oscillation searches – of measurements of (1) the absolute neutrino flux, (2) neutrino-nucleon quasi-elastic (QE) and (3) resonance (Res) interactions. In QE and Res emphasis is laid in identifying in situ measurables that help constrain nuclear effects such as initial state pair wise correlations and final state interactions.

16th International Workshop on Neutrino Factories and Future Neutrino Beam Facilities
25 -30 August, 2014
University of Glasgow, United Kingdom

*Speaker.

PoS(NUFACT2014)047

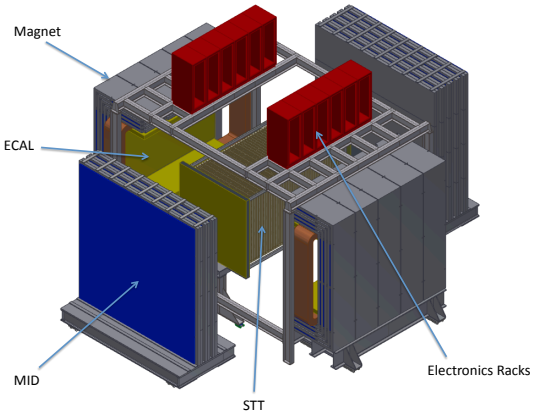

Figure 1: The LBNE near neutrino detector reference design - Fine-Grained Tracker.

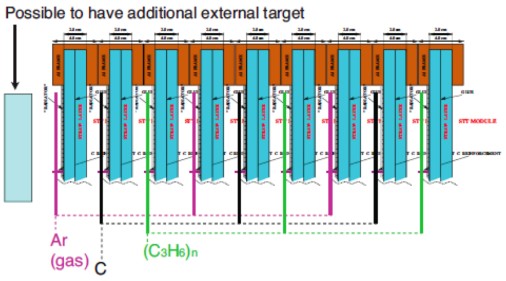

Figure 2: High-pressure argon gas targets, as well as water and other nuclear targets, are embedded in the upstream part of the tracking volume.

1. LBNE/F Near Detector

The reference design of the near detector for the LBNE experiment shown in Fig. 1 is a high-resolution Fine-Grained Tracker (FGT) capable of precisely measuring all four species of neutrinos: ν_μ, ν_e, $\bar{\nu}_\mu$ and $\bar{\nu}_e$. The FGT is composed of a $3 \times 3 \times 7.04$ m^3 Straw-Tube Tracker (STT) with transition-radiation capability surrounded by a high resolution electromagnetic calorimeter (ECAL) and embedded in a 0.4-T dipole magnet. Muon-ID detectors instrument the iron-yoke of the magnet and the downstream and upstream stations outside the magnet. The STT is instrumented with Ar and other nuclear targets as shown in Fig. 2 leading to an accurate modeling of neutrino-nucleus interactions. Table 1 summarizes the performance for the fine-grained tracker's configuration, and Table 2 lists its parameters. The goals of the FGT is to constrain the systematic errors, below the corresponding statistical error in the far detector, for all oscillation studies; and to conduct a panoply of precision measurements and searches in Neutrino physics.

In the following sections, We will present sensitivity studies – critical to constraining the systematics in oscillation searches – of measurements of (1) the absolute neutrino flux, (2) neutrino-nucleon quasi-elastic (QE) and (3) resonance (Res) interactions using a parametrized fast Monte Carlo simulation. In QE and Res emphasis is laid in identifying in situ measurables that help constrain nuclear effects such as initial state pair wise correlations and final state interactions.

2. Fast Monte Carlo

A Fast Monte Carlo simulation has been developed which combines the Geant4 LBNE beam-line flux predictions, the GENIE [2] event interaction generator, and a parameterized detector response that is used to simulate the measured (reconstructed) energy and momentum of each final-state particle. The magnetic field is simulated using the classical 4$^{\text{th}}$ order Runge-Kutta stepper which is the default method in Geant4 to compute the motion of a charged track in a general field. For charged particles, the momentum resolution is determined by $\sigma_p/p = \frac{0.05}{\sqrt{L}} + 0.008p/\sqrt{L^5}$, where p is momentum and L is track length; the angular resolution is determined

Vertex Resolution	0.1 mm
Angular Resolution	2 mrad
E_e Resolution	$6\%/\sqrt{E}$ ($\sim$4% at 3 GeV)
E_μ Resolution	3.5%
$\nu_\mu/\bar{\nu}_\mu$ ID	Yes
$\nu_e/\bar{\nu}_e$ ID	Yes
π^- .vs. π^+ ID	Yes
π^+ .vs. *proton* .vs. K^+	Yes
NCπ^0/CCe Rejection	0.1%
NCγ/CCe Rejection	0.2%
CCμ/CCe Rejection	0.01%

Table 1: Summary of the performance for the Fine-Grained Tracker configuration.

STT detector volume	$3 \times 3 \times 7.04$ m^3
STT detector mass	8 tons
Number of straws in STT	123,904
Inner magnetic volume	$4.5 \times 4.5 \times 8.0$ m^3
Targets	1.27 cm thick argon ($\sim$ 50 kg), water and others
Transition radiation radiators	2.5 cm thick
ECAL X_0	10 barrel, 10 backward, 18 forward
Number of scintillator bars in ECAL	32,320
Dipole magnet	2.4 MW power; 60 cm steel thickness
Magnetic field and uniformity	0.4 T; $< 2\%$ variation over inner volume
MuID configuration	32 RPC planes interspersed between 20 cm thick layers of steel

Table 2: Parameters for the Fine-Grained Tracker.

by $\theta_0 = \frac{13.6\text{MeV}}{\beta cp} z\sqrt{x/X_0}[1+0.038\ln(x/X_0)]$ where p, βc, and z are the momentum, velocity, and charge number of the incident particle, and x/X_0 is the thickness of the scattering medium in radiation lengths [3]. The radiation length is $X_0 = 600$ cm, and the electromagnetic and hadronic shower energy resolution are parametrized by $\sigma_E/E = 1\% + 0.06/\sqrt{E}$ and $\sigma_E/E = 1\% + 0.50/\sqrt{E}$, respectively.

3. Absolute Neutrino Flux

The high-resolution Fine-Grained Tracker can accurately measuring the un-oscillated beam flux with a precision $\leq 2\%$ for absolute normalization with neutrino-electron NC (CC) scattering.

3.1 Low-Energy Absolute Flux: Neutrino-Electron NC Scattering

Neutrino neutral current (NC) interaction with the atomic electron in the target, $\nu e^- \to \nu e^-$, provides an elegant measure of the absolute flux. The total cross section for NC elastic scattering

off atom electrons is given in Ref. [4]: The cross section of neutrino-electron neutral current is very small, $\sim 10^{-42}(E_\nu)$/GeV cm^2, which is ~2000 times smaller than that for neutrino-nucleon scattering. The cross section only depends on the precision of $\sin^2\theta_W$, for LBNE, the precision is $\leq$1%. Assuming 1.2 MW beam power, 5 tons of fiducial volume and 3 years running, the expected signal events are approximately 6,300.

The signature of neutrino-electron NC scattering is a single e^- collinear with the neutrino beam ($\leq$40 mrad). The following selection criteria are applied to select the signal and reject the background events: 1) fiducial volume, 2) one negative charged track, no positive track(s), 3) electron momentum $p_e > 0.5$ GeV, 4) electron track with minimum number of hits $n_e^{\rm hits} \geq 12$, 5) electron transverse momentum $p_e^T < 0.1$ GeV, 6) electron angle with respect to the neutrino beam $\theta_e < 0.1$ rad. The events with identified muon and/or $\pi^0/n/K_0$ will be further rejected. At the end of the selection, the signal efficiency is 73% with benign background which comes from ν_e CCQE and asymmetric conversion of a photon in an ordinary neutrino-nucleon NC events producing e^- and e^+ in equal measure with much broader angular distribution. The background can be constrained in-situ by selecting the e^+ events. There are $\sim$ 3200 neutrino-electron NC signal events passing all the selection criteria. The determination of the absolute flux is estimated to reach a precision of $\simeq$2.5% for E_ν <10 GeV, and the measurement will be dominated by the statistical error. The measurement of NC elastic scattering off electrons can only provide the integral of all neutrino flavors. Recently, MINERνA collaboration reported a precision of 13% in absolute flux determination has been achieved [5].

3.2 High-Energy Absolute Flux: Neutrino-Electron CC Scattering (IMD)

The neutrino-electron CC interaction, $\nu_l + e^- \to l^- + \nu_e$ (inverse muon decay or IMD), offers an elegant way to determine the absolute neutrino flux. The total cross section for CC elastic scattering off atom electrons is given in Ref. [4]: The threshold (for electrons at rest) $E_\nu \geq \frac{m_l^2 - m_e^2}{2m_e}$ is very high, for $l = \mu$, $E_\nu \geq 10.8$ GeV. Assuming 1.2 MW beam power, 5 tons of fiducial volume and 3 years running, the expected signal events are around 3,200.

Similiar to the neutrino-electron NC scattering, the signature of IMD is a single μ^- collinear with the neutrino beam. The following selection criteria are applied to select the signal and reject the background: 1) fiducial volume, 2) one negative charged track identified as a muon, no positive track(s), 3) muon energy $E_\mu > 10.9$ GeV, 4) muon track with minimum number of hits $n_\mu^{\rm hits} \geq 12$, 5) muon transverse momentum $p_\mu^T < 0.15$ GeV, 6) muon angle with respect to the neutrino beam $\theta_\mu < 0.005$ rad, 7) $\mathscr{Z}_\mu = E_\mu(1-\cos\theta_\mu) < 0.00025$ GeV. The events with identified $\pi^0/n/K_0$ will be further rejected. At the end of the selection, the signal efficiency is 93% with 26% background which is dominated by 1 track ν_μ CCQE. The background can be constrained in-situ using CCQE 2 track control samples, when the hadronic track is removed. The systematic limitations of CCFR [6, 7] and the CHARM-II [8] IMD measurements using the μ^+ sample can be substantially alleviated in LBNE with the proposed Fine-Grained Tracker design. There are $\sim$ 3000 neutrino-electron CC signal events passing the selection criteria, and the determination of the absolute flux is estimated to reach a precision of $\simeq$3.0% for E_ν >11 GeV.

Neutrino-electron NC (CC) scattering is a simple two-body interaction, therefore using the electron (muon) momentum and angle, we can derive the incoming neutrino energy. Figs. 3 show the comparison between the true neutrino energy (blue curve) with the derived neutrino energy

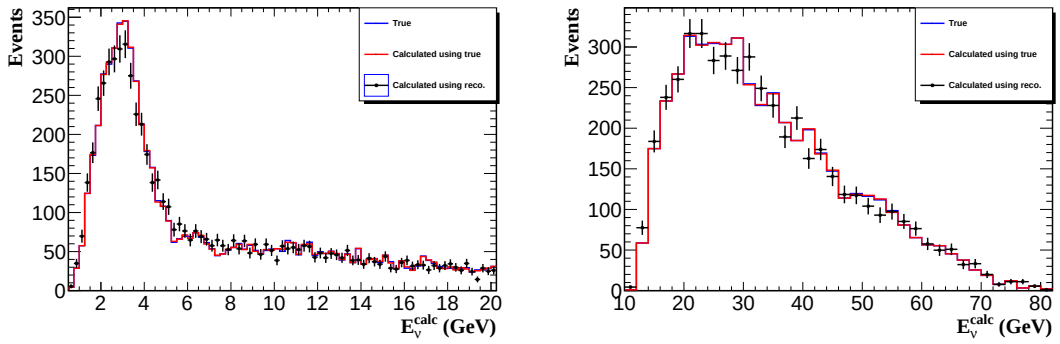

Figure 3: The derived neutrino energy using the emergent electron (left) and muon (right) momentum and angle.

(black dots) for neutrino-electron NC (left) and CC (right) scattering. The plots show that the neutrino-electron NC (CC) scattering can not only determine the neutrino absolute flux normalization to high precision, but also the flux shape.

4. Cross Sections and Nuclear Models: Charged-Current Quasi-Elastic

The Charged-Current Quasi-Elastic (CCQE) process plays an important role in the LBNE oscillation physics. Precise measurements of QE will impose direct constraints on the systematic uncertainties in neutrino-nucleon cross sections and nuclear models.

In CCQE, events will be classified as two-track sample when both muon and proton track are successfully reconstructed and one-track sample when only the muon is reconstructed. For the two-track sample, the following selection criteria are applied to select the signal and reject the background events: 1) fiducial volume 2) one negative charged track identified as a muon, 3) muon momentum $p_\mu > 0.2$ GeV, 4) muon track with minimum number of hits $n_e^{\rm hits} \geq 12$, 5) proton momentum $p_{\rm proton} > 0.1$ GeV, 6) proton track with minimum number of hits $n_{\rm proton}^{\rm hits} \geq 4$. The events with identified $\pi^0/n/K_0$ will be further rejected. At the end of the selection, the signal efficiency is 56% and the purity is 48%. The remaining event sample, composed of muon and proton, is subjected to a multivariate analysis using artificial neural network that maximizes the signal (CCQE) efficiency while keeping the Res/DIS backgrounds low by exploiting the kinematic relation between the muon and proton vectors. The energy-averaged efficiency (purity) is 48% (76%) when placing a cut at 0.45 on the multivariate distribution. Fig. 4 (left) shows the expected precision of CCQE cross section obtained in two-track analysis in brown triangle with MiniBooNE [9], NOMAD measurements [10] and the prediction from GENIE. As a a two-body interaction, the incident neutrino energy ($E_\nu^{\rm calc}$) can be derived by using the energy and angle of the muon, (E_μ and θ_μ), and compare it with the total visible energy of the two tracks, i.e., $E_{\rm vis}$ is = $E_\mu + E_{\rm proton}$; the difference between the $E_{\rm vis}$ and $E_\nu^{\rm calc}$ is, to a first approximation, the Fermi-motion. Fig. 5 (left) shows that from the fast Monte Carlo simulation.

$$E_\nu^{\rm calc} = \frac{2(M_n - E_B)E_\mu - (E_B^2 - 2M_nE_B + m_\mu^2 + \delta M^2)}{2[(M_n - E_B) - E_\mu + p_\mu \cos\theta_\mu]}, \tag{4.1}$$

where $E_\mu = T_\mu + m_\mu$ is the total muon energy and M_n, m_μ are the neutron and muon masses. Fig. 6 shows the ΔE distribution using two different nuclear models, relativistic Fermi gas model (RFGM) and spectral function (SF) (see Ref. [11] and references therein). The high-resolution Fine-Grained Tracker has the precision to tell which nuclear model describes the data and reject the wrong hypothesis.

For the one-track sample, the selection criteria are very similar to the two-track sample, but no second track. The remaining event sample, composed of single muon, is subjected to a multivariate analysis using artificial neural network. The energy-averaged efficiency (purity) is 23% (94%) when placing a cut at 0.11 on the multivariate distribution. Fig. 4 (right) shows the expected precision of CCQE cross section obtained in one-track analysis in grey triangle with MiniBooNE [9], NOMAD measurements [10] and the prediction from GENIE.

5. Cross Sections and Nuclear Models: Charged-Current Resonance

The Charge-Current Resonance (CCRes) production is the most abundant process in the LBNE energy region. In order to constraint the oscillation physics, we have to measure the resonance production precisely. CCRes provides another independent handle to constrain the nuclear effects which include initial state pair-wise correlation and final state interaction.

In this study, the three-track CCRes sample is used for the study,

$$\nu_\mu + p \to \mu^- + \Delta^{++} \to \mu^- + p + \pi^+, \tag{5.1}$$

where both proton and pion are reconstructed with an identified muon track. The following selection criteria are applied to select the signal and reject the background events: 1) fiducial volume, 2) one negative charged track identified as a muon, 3) muon momentum $p_\mu > 0.2$ GeV, 4) muon track with minimum number of hits $n_e^{\text{hits}} \geq 12$, 5) proton (pion) momentum $p_{\text{proton}(\pi^+)} > 0.1$ GeV, 6) proton (pion) track with minimum number of hits $n^{\text{hits}}_{\text{proton}(\pi^+)} \geq 4$. The events with identified $\pi^0/n/K_0$ will be further rejected. At the end of the selection, the signal efficiency is 36% and the purity is 68%. The remaining event sample, composed of muon, proton and pion, is subjected to a multivariate analysis using artificial neural network that maximizes the signal (CCQE) efficiency while keeping the DIS backgrounds low. The energy-averaged efficiency (purity) is 33% (77%) when placing a cut at 0.35 on the multivariate distribution. Fig. 4 (left) shows the expected precision of CCRes cross section obtained in three-track analysis in blue dots with Gargamelle [12], SKAT measurements [13, 14] and the prediction from GENIE.

The similar technique applied in two-track CCQE can also be used in three-track CCRes to constrain the Fermi-motion. The incident neutrino energy (E_ν^{calc}) can be derived by using the energy and angle of the muon, (E_μ and θ_μ), and compare it with the total visible energy of the two tracks, i.e., E_{vis} is $= E_\mu + E_{\text{proton}} + E_\pi$; the difference between the E_{vis} and E_ν^{calc} is, to a first approximation, the Fermi-motion. Fig. 5 (right) shows that from the fast Monte Carlo simulation.

$$E_\nu = \frac{m_\mu^2 + m_\pi^2 - 2M_p(E_\mu + E_\pi) + 2p_\mu \cdot p_\pi}{2(E_\mu + E_\pi - |\mathbf{P}_\mu|\cos\theta_\mu - |\mathbf{P}_\pi|\cos\theta_\pi - M_p)}, \tag{5.2}$$

where $E_\mu = T_\mu + m_\mu$ is the total muon energy and M_p, m_μ, m_π are the proton, muon and pion masses. By comparing this distribution to the data we can constrain the nuclear modeling in the neutrino event generator [15].

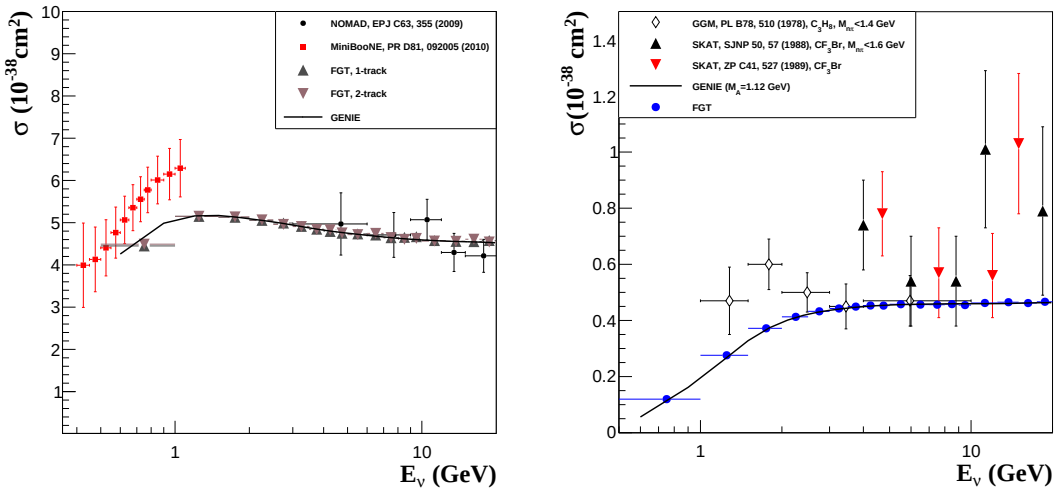

Figure 4: The expected cross section in Charged-Current Quasi-Elastic (left) and Charged-Current 3 track resonance (right).

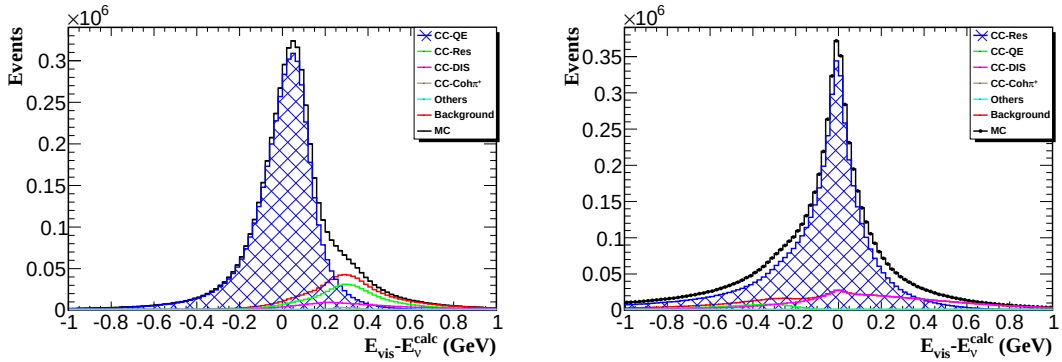

Figure 5: The distribution of ΔE in CCQE (left) and CCRes (right).

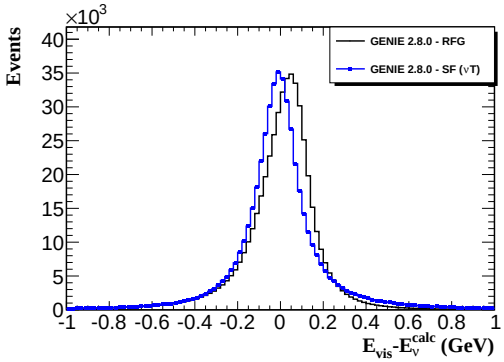

Figure 6: The distribution of ΔE with different nuclear model.

6. Conclusions

Long-Baseline Neutrino Experiment (Facility), as the third generation neutrino experiment focusing on the determination of neutrino mass hierarchy and *CP*, the control of the systematic uncertainties are the key to achieve its goal. To reach the physics objectives, in particular, sensitivity to discovery of *CP* violation, at the 5σ level, with exposures less than 500 kt.MW.years, a high-capable near detector is a must. Some preliminary studies performed show that Fine-Grained Tracker has the precision and redundancy to constrain the systematic uncertainties below the required level in beam flux, neutrino interaction modeling and detector effects. In addition, the high-resolution near detector will also independently conduct precision measurements of quantities such as neutrino-nucleon and neutrino-nuclear cross sections, electroweak parameters, sum-rules and sensitive searches for new physics, like light dark matter, with previously unachievable precision, potentially leading to additional discoveries in neutrino physics.

References

[1] C. Adams, *et al.*, *"The Long-Baseline Neutrino Experiment – Exploring Fundamental Symmetries of the Universe"*, arXiv:hep-ex/1307.7335.

[2] C. Andreopoulos, *et al.*, *Nucl. Instrum. Meth.* **A614**, 87–104 (2010), arXiv:hep-ph/0905.2517.

[3] K. A. Olive, *et al.*, *Chin. Phys. C* **38**, 090001 (2014).

[4] W. J. Marciano and Z. Parsa, *J. Phys. G*, **29**, 2629-2645 (2003), arXiv:hep-ph/0403168.

[5] J. Park, (Ph.D. Thesis), *"Direct Measurement of the NuMI Flux with Neutrino-Electron Scattering in MINERνA"*, http://lss.fnal.gov/archive/thesis/2000/fermilab-thesis-2013-36.pdf.

[6] S. Mishra, *et al.*, *Phys. Rev. Lett.* **63**, 132-135 (1989).

[7] S. Mishra, *et al.*, *Phys. Lett.* **B252**, 170-176 (1990).

[8] P. Vilian, *et al.*, *Phys. Lett.* **B364**, 121-126 (1995).

[9] A. A. Aguilar-Arevalo, *et al.* (MiniBOONE Collaboration), *Phys. Rev. D*, **81**, 092005 (2010).

[10] V. Lyubushkin, *et al.* (NOMAD Collaboration), *Eur. Phys. J.* **C63**, 355 (2009).

[11] C. -M. Jen, A. M. Ankowski, O. Benhar, A. P. Furmanski, L. N. Kalousis, and C. Mariani, *Phys. Rev. D* **90**, 093004 (2004), arXiv:hep-ex/1402.6651.

[12] W. Lerche, *et al.*, *Phys. Lett.* **B78**, 510-514 (1978).

[13] V. V. Ammosov, *et al.* (SKAT Collaboration), *Sov. J. Nucl. Phys.* **50**, 57 (1988).

[14] H. J. Grabosch, *et al.* (SKAT Collaboration), *Z. Phys.* **C41**, 527 (1989).

[15] D. Y. Hongyue, X. C. Tian, and S. R. Mishra, *"Resonance Interaction Measurement in NOMAD"*, *NUFACT 2014*, University of Glasgow, 25-30, August, 2014.